

# Heavy baryon spectrum on lattice with NRQCD bottom and HISQ lighter quarks

Protick Mohanta and Subhasish Basak

*School of Physical Sciences, National Institute of Science Education and Research, HBNI, Odisha 752050, India*

(Dated: April 23, 2020)

We determine the mass spectra of heavy baryons containing one or more bottom quarks along with their hyperfine splittings and various mass differences on MILC 2+1 Asqtad lattices at three different lattice spacings. NRQCD action is used for bottom quarks whereas relativistic HISQ action for the lighter up/down, strange and charm quarks. We consider all possible combinations of bottom and lighter quarks to construct the bottom baryon operators for the states  $J^P = 1/2^+$  and  $3/2^+$ .

## I. INTRODUCTION

Lattice QCD has been extensively employed to study  $B$  physics phenomenology, especially the decay constants and mixing parameters needed for CKM matrix elements and the mass differences in the meson sector [1]. The  $B$  mesons spectroscopy and mass splittings have undergone thorough investigations on lattice, see [1] and references therein, with increasing impact on heavy flavor phenomenology, see for instance [2]. However, studying heavy baryons with bottom quark(s) on lattice is relatively a recent pursuit. Some of the early studies of heavy baryons on lattice can be found in [3–7]. Of late, a slew of low lying  $J^P = 1/2^+$  bottom baryons, such as  $\Lambda_b$ ,  $\Sigma_b$ ,  $\Xi'_b$  and  $\Omega_b$ , have made entries in PDG [8]. Possibilities of discoveries of  $J^P = 3/2^+$  are rather high, whereas doubly and triply bottom baryons are right now beyond the reaches of present experiments. In this state, lattice QCD can provide an insight into the masses, mass splittings and other properties of such bottom baryons from the first principle. To this end, quite a few lattice investigations of heavy baryons containing one, two or three bottom quarks have been undertaken using a range of light quark actions [9–11]. For an extensive list on contemporary lattice literature on heavy baryon see [11].

These studies on heavy hadrons with bottom quark(s) are largely made possible by the use of nonrelativistic QCD action, proposed and formulated in [12, 13], because of the well-known fact that the current lattice spacings, even for as low as 0.045 fm, render  $am_b \gtrsim 1$ . Although almost all of the above studies employed different heavy quark actions for charm quark, HISQ action [14] is becoming an increasingly popular choice for the charm quark. This approach of simulating bottom quark with NRQCD and the rest of the quarks *i.e.* charm, strange and up/down with HISQ for calculation of bottom baryon spectra has been adopted in this work.

In this paper, we present our lattice QCD results of heavy baryons involving one and two bottom quarks. We consider all possible combinations of bottom quark(s) with charm, strange and up/down *lighter* quarks of the form  $(lbb)$ ,  $(llb)$  and  $(l_1l_2b)$ , where  $b$  is the bottom quark and  $l$  are the lighter charm, strange and up/down quarks. We are addressing the charm quark as “light” quark in the sense that we have used relativistic action for it. The action for the lighter quarks is HISQ [14] and NRQCD

[12, 13] for the bottom. We discuss these actions in Section II. The propagators generated using nonrelativistic and relativistic actions are required to be combined to construct baryon states of appropriate quantum numbers. A discussion to achieve this combination is spread over both Section II and III. The bottom baryon operators are described in details in Section III. In the following Section IV, we present the simulation details including the lattice ensembles used, various parameters and tuning of different quark masses. The lattice calculations are carried out at three different lattice spacings with fixed  $m_{u/d}/m_s$  value and several quark masses. We assemble our bottom baryon spectrum results along with hyperfine and various other mass splittings in the Section V. Finally we conclude and summarize in Section VI, which also includes a comparison of our results to the existing ones.

## II. QUARK ACTIONS

As of now the bottom ( $b$ ) quark masses are not small *i.e.*  $am_b \not\ll 1$  in units of the lattice spacings available. The use of improved NRQCD is the action of choice for the  $b$ -quarks. We have used  $\mathcal{O}(v^6)$  NRQCD action in this paper. The charm ( $c$ ) quark is also similarly heavy enough for existing lattices, but Fermilab proposal [15] made it possible to work with relativistic actions for  $c$ -quark, provided we trade the pole mass with the kinetic mass. Subsequently, HISQ action [14] became available for relativistic  $c$ -quark. In this paper, we choose HISQ action for the  $c$ -quark along with  $s$  and  $u/d$  quarks. In this work, as because we use the same relativistic HISQ action for all quarks except the bottom, we use the word *light* quarks to refer to  $c$ ,  $s$  and  $u/d$  quarks. This is similar to what has been done in [24] for  $B$  meson states calculation. Besides, one of the big advantages of this choice of action is the ability to use the MILC code [16] for this bit.

### A. NRQCD Action and $b$ quark

In order to perform lattice QCD computation of hadrons containing bottom quarks in publicly available relatively coarse lattices, NRQCD [12, 13] is perhaps the

most suitable and widely used quark action for bottom. As is understood, the typical velocity of a  $b$  quark inside a hadron is nonrelativistic. Comparison of masses of bottomonium states to the mass of  $b$  quark supports the fact that the velocity of  $b$  quark inside hadron ( $v^2 \sim 0.1$ ) is much smaller than the bottom mass. For example  $M_\Upsilon = 9460$  MeV whereas  $2 \times m_b = 8360$  MeV in the  $\overline{MS}$  scheme. For bottom hadrons containing lighter valence quarks, the velocity of the bottom quark is even smaller. This allows us to study the  $b$  quark with non-relativistic effective field theory. NRQCD will remain action of choice for  $b$  quark until finer lattices with  $am_b < 1$  become widely available.

In NRQCD, the upper and lower components of the Dirac spinor decouple and the  $b$  quark is described by two component spinor field, denoted by  $\psi_h$ . NRQCD Lagrangian has the following form

$$\mathcal{L} = \psi_h^\dagger(\vec{x}, t) [U_4(x) \psi_h(\vec{x}, t+1) - \psi_h(\vec{x}, t) + aH \psi_h(\vec{x}, t)] \quad (1)$$

where  $a$  is the lattice spacing and  $U_4(x)$  is the temporal gauge link operator.  $H = H_0 + \delta H$  is the NRQCD Hamiltonian where,

$$H_0 = -\frac{\tilde{\Delta}^2}{2m_b} - \frac{a}{4n} \frac{(\Delta^2)^2}{4m_b^2} \quad \text{and} \quad \delta H = \sum_i \delta H^{(i)} \quad (2)$$

The  $H_0$  is the leading  $\mathcal{O}(v^2)$  term, the  $\mathcal{O}(v^4)$  and  $\mathcal{O}(v^6)$  terms are in  $\delta H$  with coefficients  $c_1$  through  $c_7$ .

$$\begin{aligned} \delta H^{(1)} &= -c_1 \frac{(\Delta^2)^2}{8m_b^3} \\ \delta H^{(2)} &= c_2 \frac{ig}{8m_b^2} \left( \vec{\Delta}^\pm \cdot \vec{E} - \vec{E} \cdot \vec{\Delta}^\pm \right) \\ \delta H^{(3)} &= -c_3 \frac{g}{8m_b^2} \vec{\sigma} \cdot \left( \vec{\Delta}^\pm \times \vec{E} - \vec{E} \times \vec{\Delta}^\pm \right) \\ \delta H^{(4)} &= -c_4 \frac{g}{2m_b} \vec{\sigma} \cdot \vec{B} \\ \delta H^{(5)} &= -c_5 \frac{g}{8m_b^3} \left\{ \Delta^2, \vec{\sigma} \cdot \vec{B} \right\} \\ \delta H^{(6)} &= -c_6 \frac{3g}{64m_b^4} \left\{ \Delta^2, \vec{\sigma} \cdot \left( \vec{\Delta}^\pm \times \vec{E} - \vec{E} \times \vec{\Delta}^\pm \right) \right\} \\ \delta H^{(7)} &= -c_7 \frac{ig^2}{8m_b^3} \vec{\sigma} \cdot \vec{E} \times \vec{E} \end{aligned} \quad (3)$$

The  $b$  quark propagator is generated by the time evolution of this Hamiltonian,

$$\begin{aligned} G(\vec{x}, t+1; 0, 0) &= \\ &\left(1 - \frac{aH_0}{2n}\right)^n \left(1 - \frac{a\delta H}{2}\right) U_4(\vec{x}, t)^\dagger \times \\ &\left(1 - \frac{a\delta H}{2}\right) \left(1 - \frac{aH_0}{2n}\right)^n G(\vec{x}, t; 0, 0) \end{aligned} \quad (4)$$

with

$$G(\vec{x}, t; 0, 0) = \begin{cases} 0 & \text{for } t < 0 \\ \delta_{\vec{x}, 0} & \text{for } t = 0 \end{cases}$$

The tree level value of all the coefficients  $c_1, c_2, c_3, c_4, c_5, c_6$  and  $c_7$  is 1. Here  $n$  is the factor introduced to ensure numerical stability at small  $am_b$  [13], where  $n > 3/2m_b$ . The symmetric derivative  $\Delta^\pm$  and Laplacian  $\Delta^2$  in terms of forward and backward covariant derivatives are

$$\begin{aligned} a\Delta_\mu^+ \psi(x) &= U_\mu(x) \psi(x + a\hat{\mu}) - \psi(x) \\ a\Delta_\mu^- \psi(x) &= \psi(x) - U_\mu^\dagger(x - a\hat{\mu}) \psi(x - a\hat{\mu}) \\ \Delta^\pm &= \frac{1}{2} (\Delta^+ + \Delta^-) \\ \Delta^2 &= \sum_i \Delta_i^+ \Delta_i^- = \sum_i \Delta_i^- \Delta_i^+ \end{aligned} \quad (5)$$

By Taylor expanding the symmetric derivative and the Laplacian operator, we can find their forms corrected up to  $\mathcal{O}(a^4)$  [12] that are used in the above Equation (3).

$$\begin{aligned} \tilde{\Delta}_i^\pm &= \Delta_i^\pm - \frac{a^2}{6} \Delta_i^+ \Delta_i^\pm \Delta_i^- \\ \tilde{\Delta}^2 &= \Delta^2 - \frac{a^2}{12} \sum_i [\Delta_i^+ \Delta_i^-]^2. \end{aligned} \quad (6)$$

In the same way, the gauge fields are improved to  $\mathcal{O}(a^4)$  using cloverleaf plaquette,

$$\begin{aligned} a\Delta_\rho^+ F_{\mu\nu}(x) &= U_\rho(x) F_{\mu\nu}(x + a\hat{\rho}) U_\rho^\dagger(x) - F_{\mu\nu}(x) \\ a\Delta_\rho^- F_{\mu\nu}(x) &= F_{\mu\nu}(x) - U_\rho^\dagger(x - a\hat{\rho}) F_{\mu\nu}(x) U_\rho(x - a\hat{\rho}) \\ g\tilde{F}_{\mu\nu}(x) &= gF_{\mu\nu}(x) - \frac{a^4}{6} [\Delta_\mu^+ \Delta_\mu^- + \Delta_\nu^+ \Delta_\nu^-] gF_{\mu\nu}(x) \end{aligned} \quad (7)$$

The chromo-electric  $\tilde{E}$  and chromo-magnetic  $\tilde{B}$  fields in  $\delta H^{(3)}$  and  $\delta H^{(4)}$  of Equation (3) are thus  $\mathcal{O}(a^4)$  improved.

## B. HISQ charm and lighter quarks

For the lighter quarks – charm, strange and up/down – relativistic HISQ action [14] is used. Apart from anything else, from practical point of coding the bottom-light operators ( $lbb, llb, l_1l_2b$ ), using the same relativistic action for all lighter quarks offers a great degree of simplification. The HISQ action is given by,

$$\mathcal{S} = \sum_x \bar{l}(x) (\gamma^\mu D_\mu^{\text{HISQ}} + m) l(x) \quad (8)$$

where,

$$D_\mu^{\text{HISQ}} = \Delta_\mu(W) - \frac{a^2}{6} (1 + \epsilon) \Delta_\mu^3(X) \quad (9)$$

with  $W_\mu(x) = F_\mu^{\text{HISQ}} U_\mu(x)$  and  $X_\mu(x) = \mathcal{U} F_\mu U_\mu(x)$ . The  $F_\mu^{\text{HISQ}}$  has the form

$$F_\mu^{\text{HISQ}} = \left( F_\mu - \sum_{\rho \neq \mu} \frac{a^2 (\delta_\rho)^2}{2} \right) \mathcal{U} F_\mu \quad (10)$$

Here the  $\mathcal{U}$  is the unitarizing operator, it unitarizes whatever it acts on and the smearing operator  $F_\mu$  is given by

$$F_\mu = \prod_{\rho \neq \mu} \left( 1 + \frac{a^2 \delta_\rho^{(2)}}{4} \right). \quad (11)$$

The  $\delta_\rho$  and  $\delta_\rho^{(2)}$  in the Equations (10) and (11) are covariant first and second order derivatives. Because HISQ action reduces  $\mathcal{O}(\alpha_s a^2)$  discretization errors found in Asqtad action, it is well suited for  $s$  and  $u/d$  quarks. The parameter  $\epsilon$  in the coefficient of Naik term can be appropriately tuned to use the action for  $c$  quark. For  $s$  and  $u/d$  quarks, the  $\epsilon = 0$ . Later, in the Table IV we listed the parameters used for HISQ quarks. We have taken the values of  $\epsilon$  from [24] and used MILC subroutines for generating HISQ propagators.

Since HISQ action is diagonal in spin space, propagators obtained do not have any spin structure. The full  $4 \times 4$  spin structure can be regained by multiplying the propagators by Kawamoto-Smit multiplicative phase factor [19],

$$\Omega(x) = \prod_{\mu=1}^4 (\gamma_\mu)^{x_\mu} = \gamma_1^{x_1} \gamma_2^{x_2} \gamma_3^{x_3} \gamma_4^{x_4}. \quad (12)$$

MILC library uses a different representation of  $\gamma$  matrices than the ones used in NRQCD. However,  $\gamma$  matrices of these two representations are related by the unitary transformation of the form

$$S \gamma_\mu^{\text{MILC}} S^\dagger = \gamma_\mu^{\text{NR}} \quad \text{where, } S = \frac{1}{\sqrt{2}} \begin{pmatrix} \sigma_y & \sigma_y \\ -\sigma_y & \sigma_y \end{pmatrix} \quad (13)$$

### III. TWO-POINT FUNCTIONS

In this section we discuss the construction of the bottom baryons by combining spin and color indices of the appropriate quark fields to form necessary baryon operators and two-point functions. The  $b$  quark field is universally represented with  $Q$  throughout the paper. It is defined later in the Equation (17).

#### A. Bottom-bottom meson two-point function

After the  $b$  quark propagators are generated according to Equation (4), we calculate the masses of bottomonium states from the exponential fall-off of two-point functions *i.e.* correlators of the state with quantum numbers of interest. The meson creation operators are constructed from two component quark and anti-quark creation operators  $\psi_h^\dagger$  and  $\chi_h^\dagger$  [17, 18]. As antiquarks transform as  $\bar{3}$  under color rotation, we rename the antiquark spinor as  $\chi_h \equiv \chi_h^*$  [13]. The meson creation operator is thus,

$$\mathcal{O}_{hh}(x) = \psi_h^\dagger(x) \Gamma \chi_h(x). \quad (14)$$

Heavy-heavy *i.e.* bottom-bottom meson two-point function is then given by [13, 20],

$$\begin{aligned} C_{hh}(\vec{p}, t) &= \sum_{\vec{x}} \langle \mathcal{O}_{hh}^\dagger(x) \mathcal{O}_{hh}(0) \rangle \\ &= \sum_{\vec{x}} e^{i\vec{p} \cdot \vec{x}} \text{Tr} \left[ G^\dagger(x, 0) \Gamma_{\text{sink}}^\dagger G(x, 0) \Gamma_{\text{src}} \right] \end{aligned} \quad (15)$$

$\Gamma_{\text{sink}} = \Gamma_{\text{src}} = I$  and  $\sigma_i$  for the pseudoscalar and vector mesons respectively. Heavy-heavy propagator  $G(x, 0)$  is a  $2 \times 2$  matrix in spin space. If we think  $G(x, 0)$  as a  $4 \times 4$  matrix with vanishing lower components then we can rewrite the above Equation (15) as [9]

$$C_{hh}(\vec{p}, t) = \sum_{\vec{x}} e^{i\vec{p} \cdot \vec{x}} \text{Tr} \left[ \gamma_5 G^\dagger(x, 0) \gamma_5 \Gamma_{\text{sink}}^\dagger G(x, 0) \Gamma_{\text{src}} \right] \quad (16)$$

where  $\Gamma$  matrices now changed to  $\Gamma_{\text{sink}} = \Gamma_{\text{src}} = \gamma_5$  and  $\gamma_i$  for pseudoscalar and vector mesons respectively. In Equation (16) we have used the non-relativistic Dirac representation of  $\gamma$  matrices. In the Equations (15), (16) and (19) the trace is taken over both the spin and color indices.

#### B. Heavy-light meson two-point function

As discussed above,  $b$  quark field  $\psi_b$  has only two spin components. We convert it to a 4-component spinor having vanishing lower components

$$Q = \begin{pmatrix} \psi_b \\ 0 \end{pmatrix} \quad (17)$$

This helps us to combine the  $b$  and light quark fields in the usual way,

$$\mathcal{O}_{hl}(x) = \bar{Q}(x) \Gamma l(x) \quad (18)$$

where  $l(x)$  stands for the light quark fields,  $\bar{Q} = Q^\dagger \gamma_4$  and depending on pseudoscalar and vector mesons  $\Gamma = \gamma_5$  and  $\gamma_i$  respectively. Note that in the Dirac *i.e.* NR representation of  $\gamma$ -matrices  $\gamma_4 Q = Q$ . The zero momentum bottom-light two-point function becomes [10, 30],

$$\begin{aligned} C_{hl}(t) &= \sum_{\vec{x}} \langle \mathcal{O}_{hl}^\dagger(x) \mathcal{O}_{hl}(0) \rangle \\ &= \sum_{\vec{x}} \text{Tr} \left[ \gamma_5 M^\dagger(x, 0) \gamma_5 \Gamma_{\text{sink}}^\dagger G(x, 0) \Gamma_{\text{src}} \right] \end{aligned} \quad (19)$$

where  $M(x, 0)$  is the light quark propagator. It has the usual full  $4 \times 4$  spin structure. As before,  $G(x, 0)$  is the  $b$  quark propagator having vanishing lower components. However, before implementing Equation (19),  $G(x, 0)$  has to be rotated to the MILC basis.

### C. Bottom baryon two-point functions

The bottom quark field  $Q$  has vanishing lower components and hence can be projected to positive parity states only. Besides, the use of  $\Gamma = C\gamma_5$  in a diquark operator made from same flavor *i.e.*  $l^T C\gamma_5 l$  is not allowed by Pauli exclusion principle. In other words, the insertion of  $C\gamma_5$  between two quark fields of same flavor creates a combination which is antisymmetric in spin indices, while the presence of  $\epsilon_{abc}$  makes the combination antisymmetric in color indices. This makes the overall operator become symmetric under the interchange of the same flavored quark fields. Keeping this in mind, the constructions of various bottom baryon two-point functions are described below.

**Triply bottom baryon:** Triply bottom baryon operator is defined by

$$(\mathcal{O}_k^{hhh})_\alpha = \epsilon_{abc} \left( Q^{aT} C \gamma_k Q^b \right) Q_\alpha^c \quad (20)$$

where  $C = \gamma_4 \gamma_2$ . Here  $a, b, c$  are the color indices,  $\alpha$  is the spinor index and  $k$  is the Lorentz index which runs from 1 to 3. The zero momentum two-point function reads [9]

$$\begin{aligned} C_{jk;\alpha\delta}^{hhh}(t) &= \sum_{\vec{x}} \left\langle [\mathcal{O}_j^{hhh}(x)]_\alpha [\mathcal{O}_k^{hhh}(0)]_\delta^\dagger \right\rangle \\ &= \sum_{\vec{x}} \epsilon_{abc} \epsilon_{fgh} G_{\alpha\delta}^{ch}(x, 0) \times \\ &\quad \text{Tr} \left[ C \gamma_j G^{bg}(x, 0) \gamma_k \gamma_2 G^{afT}(x, 0) \right] \end{aligned} \quad (21)$$

In the above Equation (21) and the subsequent ones, the transpose and traces are taken over spin indices. Baryon operators having  $C\gamma_k$  in the diquark component have overlap with both spin- $\frac{3}{2}$  and  $\frac{1}{2}$  states. For example, correlator defined in Equation (21) can be written explicitly as an overlap with both spin- $\frac{3}{2}$  and  $\frac{1}{2}$  states [31],

$$C_{ij}^{hhh}(t) = Z_{3/2}^2 e^{-E_{3/2}t} \Pi P_{ij}^{3/2} + Z_{1/2}^2 e^{-E_{1/2}t} \Pi P_{ij}^{1/2} \quad (22)$$

where  $\Pi = (1 + \gamma_4)/2$  and the spin projection operators  $P_{ij}^{3/2} = \delta_{ij} - \gamma_i \gamma_j / 3$  and  $P_{ij}^{1/2} = \gamma_i \gamma_j / 3$ . The individual contribution to the respective spin states can be obtained by taking appropriate projections,

$$\begin{aligned} P_{ij}^{3/2} C_{jk}^{hhh} &= Z_{3/2}^2 \Pi e^{-E_{3/2}t} P_{ik}^{3/2} \\ P_{ij}^{1/2} C_{jk}^{hhh} &= Z_{1/2}^2 \Pi e^{-E_{1/2}t} P_{ik}^{1/2} \end{aligned} \quad (23)$$

In this paper, we use these projections to separate the different spin states. We would like to point out that the spin- $\frac{1}{2}$  state of triply bottom baryon is not a physical state as it violates Pauli exclusion principle even though we can take the projection in practice.

**Bottom-bottom-light baryon:** Interpolating operator for baryons, having two  $b$  quarks and a light quark, can

be constructed in two ways based on how the diquark component is formed [32].

$$(\mathcal{O}_k^{hhl})_\alpha = \epsilon_{abc} \left( Q^{aT} C \gamma_k Q^b \right) l_\alpha^c \quad (24)$$

$$(\mathcal{O}_k^{hh})_\alpha = \epsilon_{abc} \left( Q^{aT} C \gamma_k l^b \right) Q_\alpha^c \quad (25)$$

The corresponding baryon correlators are

$$\begin{aligned} C_{jk;\alpha\delta}^{hhl}(t) &= \sum_{\vec{x}} \left\langle [\mathcal{O}_j^{hhl}(x)]_\alpha [\mathcal{O}_k^{hhl}(0)]_\delta^\dagger \right\rangle \\ &= \sum_{\vec{x}} \epsilon_{abc} \epsilon_{fgh} [M^{ch}(x, 0) \gamma_4]_{\alpha\delta} \times \\ &\quad \text{Tr} \left[ \gamma_4 \gamma_2 \gamma_j G^{bg}(x, 0) \gamma_k \gamma_2 G^{afT}(x, 0) \right] \end{aligned} \quad (26)$$

$$\begin{aligned} C_{jk;\alpha\delta}^{hh}(t) &= \sum_{\vec{x}} \left\langle [\mathcal{O}_j^{hh}(x)]_\alpha [\mathcal{O}_k^{hh}(0)]_\delta^\dagger \right\rangle \\ &= \sum_{\vec{x}} \epsilon_{abc} \epsilon_{fgh} G_{\alpha\delta}^{ch}(x, 0) \times \\ &\quad \text{Tr} \left[ \gamma_4 \gamma_2 \gamma_j M^{bg}(x, 0) \gamma_k \gamma_2 G^{afT}(x, 0) \right] \end{aligned} \quad (27)$$

The propagator  $G(x, 0)$  is required to be converted to MILC basis using the unitary matrix  $S$  defined in Equation (13).

An additional spin- $\frac{1}{2}$  operator can be defined for the  $\mathcal{O}^{hhl}$  type operator as

$$(\mathcal{O}_5^{hhl})_\alpha = \epsilon_{abc} \left( Q^{aT} C \gamma_5 l^b \right) Q_\alpha^c \quad (28)$$

The two-point function for this operator is obtained by replacing  $\gamma_j$  and  $\gamma_k$  by  $\gamma_5$  in Equation (27). We cannot have a  $C\gamma_5$  between two  $Q$  in diquark and hence no  $\mathcal{O}_5^{hhl}$ .

TABLE I. Operators for triple and double bottom baryons.  $Q$  is used for  $b$  field and  $l$  for any of the  $c, s, u/d$  lighter quarks.

Baryon	Quark content	$J^P$	Operator
$\Omega_{bbb}$	$bbb$	$\frac{3}{2}^+, \frac{1}{2}^+$	$\epsilon_{abc} (Q^{aT} C \gamma_k Q^b) Q^c$
$\Omega_{cbb}^*, \Omega_{cbb}$	$cbb$	$\frac{3}{2}^+, \frac{1}{2}^+$	$\epsilon_{abc} (Q^{aT} C \gamma_k Q^b) l^c$
$\tilde{\Omega}_{cbb}^*, \tilde{\Omega}_{cbb}$	$cbb$	$\frac{3}{2}^+, \frac{1}{2}^+$	$\epsilon_{abc} (Q^{aT} C \gamma_k l^b) Q^c$
$\Omega'_{cbb}$	$cbb$	$\frac{1}{2}^+$	$\epsilon_{abc} (Q^{aT} C \gamma_5 l^b) Q^c$
$\Omega_{bb}^*, \Omega_{bb}$	$sbb$	$\frac{3}{2}^+, \frac{1}{2}^+$	$\epsilon_{abc} (Q^{aT} C \gamma_k Q^b) l^c$
$\tilde{\Omega}_{bb}^*, \tilde{\Omega}_{bb}$	$sbb$	$\frac{3}{2}^+, \frac{1}{2}^+$	$\epsilon_{abc} (Q^{aT} C \gamma_k l^b) Q^c$
$\Omega'_{bb}$	$sbb$	$\frac{1}{2}^+$	$\epsilon_{abc} (Q^{aT} C \gamma_5 l^b) Q^c$
$\Xi_{bb}^*, \Xi_{bb}$	$ubb$	$\frac{3}{2}^+, \frac{1}{2}^+$	$\epsilon_{abc} (Q^{aT} C \gamma_k Q^b) l^c$
$\tilde{\Xi}_{bb}^*, \tilde{\Xi}_{bb}$	$ubb$	$\frac{3}{2}^+, \frac{1}{2}^+$	$\epsilon_{abc} (Q^{aT} C \gamma_k l^b) Q^c$
$\Xi'_{bb}$	$ubb$	$\frac{1}{2}^+$	$\epsilon_{abc} (Q^{aT} C \gamma_5 l^b) Q^c$

In Table I we tabulated the full list of triple and double bottom baryon operators that are used in this work. We have broadly followed the nomenclature

adopted in [11] but with certain modifications as needed for this work. The baryons having the same quark content and  $J^P$  are obtained in two different ways, as mentioned above. The operators with “tilde”, for instance  $\tilde{\Omega}_{bb}$  ( $1/2^+$ ), are obtained by projecting the relevant  $(QC\gamma_k l)Q$  operator with  $P_{ij}^{1/2}$ . The operators with “prime”, such as  $\Omega'_{bb}$  ( $1/2^+$ ), are obtained from  $(QC\gamma_5 l)Q$  diquark construction. The “prime” states so constructed on lattice correspond to the “prime” continuum states, such as  $\Xi'_b$  or till unobserved  $\Omega'_{cb}$  etc. It is obvious that baryon states calculated by projecting out definite spin states from a two-point function share the same interpolating operator. The star-ed baryons are for  $J^P = 3/2^+$  states.

**Bottom-light-light baryon:** The natural choice for interpolating operator, as motivated by Heavy Quark Effective Theory [34], in  $llh$ -baryon kind is

$$(\mathcal{O}_k^{hl_1 l_2})_\alpha = \epsilon_{abc} (l_1^{aT} C \gamma_k l_2^b) Q_\alpha^c \quad (29)$$

and the corresponding two-point function is

$$\begin{aligned} C_{jk;\alpha\delta}^{hl_1 l_2}(t) &= \sum_{\vec{x}} \langle [\mathcal{O}_j^{hl_1 l_2}(x)]_\alpha [\mathcal{O}_k^{hl_1 l_2}(0)]_\delta^\dagger \rangle \\ &= \sum_{\vec{x}} \epsilon_{abc} \epsilon_{fgh} G_{\alpha\delta}^{ch}(x, 0) \times \\ &\quad \text{Tr} \left[ \gamma_4 \gamma_2 \gamma_j M_2^{bg}(x, 0) \gamma_k \gamma_2 \gamma_4 M_1^{afT}(x, 0) \right] \end{aligned} \quad (30)$$

In HISQ formalism for light quarks, the corresponding propagators  $M_1(x, 0)$  and  $M_2(x, 0)$  have the same Kawamoto-Smit multiplicative factor  $\Omega(x)$ . Hence they have the same spin structure irrespective of color indices. As a result, the trace over spin indices in Equation (30) vanishes if  $\gamma_j \neq \gamma_k$ . Therefore, we can not separate the two spin- $\frac{3}{2}$  and  $\frac{1}{2}$  states. If we want to use the same diquark structure as in Equation (29), for baryons having different light quark flavors we can define the spin- $\frac{1}{2}$  operator by

$$(\mathcal{O}_5^{hl_1 l_2})_\alpha = \epsilon_{abc} (l_1^{aT} C \gamma_5 l_2^b) Q_\alpha^c \quad (31)$$

and the corresponding two-point function is

$$\begin{aligned} C_{55;\alpha\delta}^{hl_1 l_2}(t) &= \sum_{\vec{x}} \langle [\mathcal{O}_5^{hl_1 l_2}(x)]_\alpha [\mathcal{O}_5^{hl_1 l_2}(0)]_\delta^\dagger \rangle \\ &= \sum_{\vec{x}} \epsilon_{abc} \epsilon_{fgh} G_{\alpha\delta}^{ch}(x, 0) \times \\ &\quad \text{Tr} \left[ \gamma_4 \gamma_2 \gamma_5 M_2^{bg}(x, 0) \gamma_5 \gamma_2 \gamma_4 M_1^{afT}(x, 0) \right] \end{aligned} \quad (32)$$

Besides, instead of Equation (29), we can choose our  $(hl_1 l_2)$ -operator as

$$(\mathcal{O}_k^{hl_2 l_1})_\alpha = \epsilon_{abc} (Q^{aT} C \gamma_k l_2^b) l_{1\alpha}^c \quad (33)$$

The two-point function is now

$$\begin{aligned} C_{jk;\alpha\delta}^{hl_2 l_1}(t) &= \sum_{\vec{x}} \epsilon_{abc} \epsilon_{fgh} [M_1^{ch}(x, 0) \gamma_4]_{\alpha\delta} \times \\ &\quad \text{Tr} \left[ \gamma_4 \gamma_2 \gamma_j M_2^{bg}(x, 0) \gamma_k \gamma_2 G^{afT}(x, 0) \right] \end{aligned} \quad (34)$$

Because the light quark propagators  $M_1(x, 0)$  and  $M_2(x, 0)$  are proportional to each other, the relative positions of the quark fields  $l_1$  and  $l_2$  in Equation (33) is irrelevant. Interpolating operator defined in Equation (33) has overlap with both spin- $\frac{3}{2}$  and  $\frac{1}{2}$  states and can be projected out by appropriate projection operators  $P_{ij}^{1/2, 3/2}$ .

As before, we can also define an additional spin- $\frac{1}{2}$  operator here too,

$$(\mathcal{O}_5^{hl_2 l_1})_\alpha = \epsilon_{abc} (Q^{aT} C \gamma_5 l_2^b) l_{1\alpha}^c \quad (35)$$

The two-point function for this operator has the same form as in Equation (34) with  $\gamma_j$  and  $\gamma_k$  replaced by  $\gamma_5$ .

TABLE II. Operators for single bottom baryons.  $Q$  is used for  $b$  field as before. Interchange in the position of two lighter quarks keeps the operator unchanged.

Baryon	Quark content	$J^P$	Operator
$\tilde{\Omega}_{ccb}^*, \tilde{\Omega}_{ccb}$	$ccb$	$\frac{3}{2}^+, \frac{1}{2}^+$	$\epsilon_{abc} (Q^{aT} C \gamma_k c^b) c^c$
$\Omega'_{ccb}$	$ccb$	$\frac{1}{2}^+$	$\epsilon_{abc} (Q^{aT} C \gamma_5 c^b) c^c$
$\Omega_{cb}$	$scb$	$\frac{1}{2}^+$	$\epsilon_{abc} (s^{aT} C \gamma_5 c^b) Q^c$
$\tilde{\Omega}_{cb}^*, \tilde{\Omega}_{cb}$	$scb$	$\frac{3}{2}^+, \frac{1}{2}^+$	$\epsilon_{abc} (Q^{aT} C \gamma_k c^b) s^c$
$\Omega'_{cb}$	$scb$	$\frac{1}{2}^+$	$\epsilon_{abc} (Q^{aT} C \gamma_5 c^b) s^c$
$\Xi_{cb}$	$ucb$	$\frac{1}{2}^+$	$\epsilon_{abc} (u^{aT} C \gamma_5 c^b) Q^c$
$\tilde{\Xi}_{cb}^*, \tilde{\Xi}_{cb}$	$ucb$	$\frac{3}{2}^+, \frac{1}{2}^+$	$\epsilon_{abc} (Q^{aT} C \gamma_k c^b) u^c$
$\Xi'_{cb}$	$ucb$	$\frac{1}{2}^+$	$\epsilon_{abc} (Q^{aT} C \gamma_5 c^b) u^c$
$\tilde{\Omega}_b^*, \tilde{\Omega}_b$	$ssb$	$\frac{3}{2}^+, \frac{1}{2}^+$	$\epsilon_{abc} (Q^{aT} C \gamma_k s^b) s^c$
$\Omega'_b$	$ssb$	$\frac{1}{2}^+$	$\epsilon_{abc} (Q^{aT} C \gamma_5 s^b) s^c$
$\Xi_b$	$usb$	$\frac{1}{2}^+$	$\epsilon_{abc} (u^{aT} C \gamma_5 s^b) Q^c$
$\tilde{\Xi}_b^*, \tilde{\Xi}_b$	$usb$	$\frac{3}{2}^+, \frac{1}{2}^+$	$\epsilon_{abc} (Q^{aT} C \gamma_k s^b) u^c$
$\Xi'_b$	$usb$	$\frac{1}{2}^+$	$\epsilon_{abc} (Q^{aT} C \gamma_5 s^b) u^c$
$\tilde{\Sigma}_b^*, \tilde{\Sigma}_b$	$uub$	$\frac{3}{2}^+, \frac{1}{2}^+$	$\epsilon_{abc} (Q^{aT} C \gamma_k u^b) u^c$
$\Sigma'_b$	$uub$	$\frac{1}{2}^+$	$\epsilon_{abc} (Q^{aT} C \gamma_5 u^b) u^c$
$\Lambda_b$	$udb$	$\frac{1}{2}^+$	$\epsilon_{abc} (u^{aT} C \gamma_5 d^b) Q^c$

In Table II we tabulate our full list of single bottom baryon operators that we made use of in this work. The “tilde” and “prime” states that appear in the table have been explained before in the context of multi bottom baryon operators.

**Light baryon:** We occasionally need charmed baryon states like  $qcc$  or  $qqc$ , where  $q$  is any of  $s$  or  $u/d$  quarks or both, hence we include a discussion on charmed baryon operators. The  $c$ -quark in the present case is relativistic. For the reason discussed above, with HISQ action for

lighter quarks we can define only the spin- $\frac{1}{2}$  operators. Consider a  $(l_1 l_2 l_3)$ -baryon where at least two quarks are differently flavored, say  $l_1 \neq l_2$ . The spin- $\frac{1}{2}$  operator and the corresponding two-point function in such case is

$$(\mathcal{O}_5^{l_1 l_2 l_3})_\alpha = \epsilon_{abc} (l_1^{aT} C \gamma_5 l_2^b) l_{3\alpha}^c \quad (36)$$

$$C_{55, \alpha\delta}^{l_1 l_2 l_3}(t) = \sum_{\vec{x}} \epsilon_{abc} \epsilon_{fgh} [M_3^{ch}(x, 0) \gamma_4]_{\alpha\delta} \times \\ \text{Tr} \left[ \gamma_4 \gamma_2 \gamma_5 M_2^{bg}(x, 0) \gamma_5 \gamma_2 \gamma_4 M^{afT}_1(x, 0) \right] \quad (37)$$

The two light baryon states ( $J^P = 1/2^+$ ) that we are interested in this work are,

$$\begin{aligned} \Sigma_c(uuc) : & \quad \epsilon_{abc} (c^{aT} C \gamma_5 u^b) u^c \\ \Xi_{cc}(ucc) : & \quad \epsilon_{abc} (c^{aT} C \gamma_5 u^b) c^c \end{aligned} \quad (38)$$

#### IV. SIMULATION DETAILS

We calculated the bottom baryon spectra using the publicly available  $N_f = 2 + 1$  Asqtad gauge configurations generated by MILC collaboration. Details about these lattices can be found in [21]. It uses Symanzik-improved Lüscher-Weisz action for the gluons and Asqtad action [22, 23] for the sea quarks. The lattices we choose have a fixed ratio of  $am_l/am_s = 1/5$  and lattice spacings ranging from 0.15 fm to 0.09 fm corresponding to the same physical volume. We have not determined the lattice spacings independently but use those given in [21]. In Table III we listed the ensembles used in this work.

TABLE III. MILC configurations used in this work. The gauge coupling is  $\beta$ , lattice spacing  $a$ ,  $u/d$  and  $s$  sea quark masses are  $m_l$  and  $m_s$  respectively and lattice size is  $L^3 \times T$ . The  $N_{\text{cfg}}$  is number of configurations used in this work.

$\beta = 10/g^2$	$a(\text{fm})$	$am_l$	$am_s$	$L^3 \times T$	$N_{\text{cfg}}$
6.572	0.15	0.0097	0.0484	$16^3 \times 48$	400
6.76	0.12	0.01	0.05	$20^3 \times 64$	400
7.09	0.09	0.0062	0.031	$28^3 \times 96$	300

In NRQCD the rest mass term does not appear in Equation (3) and therefore we cannot determine hadron masses from their energies at zero momentum directly from the exponential fall-off of the correlation functions. Instead, we calculate the kinetic mass  $M_k$  of heavy-heavy mesons from its energy-momentum relation, which to  $\mathcal{O}(p^2)$  is [15],

$$\begin{aligned} E(p) &= E(0) + \sqrt{p^2 + M_k^2} - M_k \\ \Rightarrow E(p)^2 &= E(0)^2 + \frac{E(0)}{M_k} p^2 \end{aligned} \quad (39)$$

We calculate the  $E(p)$  at different values of lattice momenta  $p = 2n\pi/L$  where,  $n = (0,0,0), (1,0,0), (1,1,0),$

$(1,1,1), (2,0,0), (2,1,0)$  and  $(2,1,1)$ .

**$m_b$  tuning:** The  $b$  quark mass is tuned from the spin average  $\Upsilon$  and  $\eta_b$  masses

$$M_{b\bar{b}} = \frac{3M_\Upsilon + M_{\eta_b}}{4} \quad (40)$$

using kinetic mass for both  $\Upsilon$  and  $\eta_b$ . The experimental value to which  $M_{b\bar{b}}$  is tuned to is not 9443 MeV, as obtained from spin averaging  $\Upsilon$  (9460 MeV) and  $\eta_b$  (9391 MeV) experimental masses, but to an appropriately adjusted value of 9450 MeV [24], which we denote as  $M_{\text{phys}}^{\text{mod}}$  later in the Equation (41). The reasons being, firstly electromagnetic interaction among the quarks are not considered here. Secondly, the disconnected diagrams while computing two-point function are also not considered thus not allowing  $b, \bar{b}$  quarks to annihilate to gluons. And finally, we do not have sea  $c$  quarks in our simulation. For a more detailed discussion on this, see [24].

The  $b$  quark mass  $m_b$  and the coefficient  $c_4$  in Equation (3) are then tuned to obtain modified spin average mass and the hyperfine splitting of  $\Upsilon$  and  $\eta_b$ , which is  $\sim 60 - 65$  MeV [25]. In order to achieve the desired hyperfine splittings, we tuned only  $c_4$  since at  $\mathcal{O}(1/m_b)$  this is the only term that contains Pauli spin matrices. Therefore, it allows the mixing of spin components of  $\psi_h$ . This term contributes maximally to the hyperfine splitting compared to the others that contain Pauli spin matrices. The one-loop radiative correction to  $c_4$  [26] has been used to tune hyperfine splitting in [27] where it was found to change, but only mildly, over lattice spacings  $\sim 0.15 - 0.09$  fm for  $N_f = 2 + 1 + 1$  HISQ gauge configurations. In our present mixed action study, the changes in the tuned  $c_4$  on various lattice ensembles are small enough. Taking an average of those values we choose  $c_4 = 1.9$  for which the hyperfine splittings obtained on three different lattices 0.15, 0.12 and 0.09 fm are 60.6 MeV, 61.1 MeV and 61.8 MeV respectively.

All other coefficients  $c_i$  in Equation (3) are set to 1.0. We set stability factor  $n = 4$  throughout our simulation. The Table IV lists the values of  $m_b$  used in this work.

TABLE IV. Tuned  $b, c$  and  $s$  quark bare masses for lattices used in this work. For  $s$ -quark mass, we mentioned the particle states to which it is tuned to. The values of  $\epsilon$ -parameter used for  $c$ -quark are given in the last column.

$a$ (fm)	$am_b$	$am_c$	$am_s$ ( $\eta_s$ )	$am_s$ ( $B_s$ )	$\epsilon$ [24]
0.15	2.76	0.850	0.065	0.215	-0.34
0.12	2.08	0.632	0.049	0.155	-0.21
0.09	1.20	0.452	0.0385	0.114	-0.115

**$m_c$  tuning:** The  $c$ -quark mass is tuned pretty much in the same way as  $m_b$ , except that  $M_{cc}$  is tuned to the spin average of  $J/\psi$  and  $\eta_c$  experimental masses. In this case,

however, the adjustment to spin averaged value due to the absence of electromagnetic interaction,  $c$ -quarks in sea and disconnected diagrams are very small and hence neglected. The bare  $c$ -quark masses used in this work are given in Table IV.

**$m_s$  tuning:** The  $s$ -quark mass is tuned to two different values. In the first case, we tune to the mass of fictitious  $s\bar{s}$  pseudoscalar meson  $\eta_s$  while in the second case to the mass of  $B_s$ . The  $\eta_s$  is a fictitious meson that is not allowed to decay through  $s\bar{s}$  annihilation. Hence no disconnected diagrams arise in the two-point function calculation. From chiral perturbation theory, its mass is estimated to be  $m_{\eta_s} = \sqrt{2m_K^2 - m_\pi^2} = 689$  MeV [28, 29]. The  $s$ -quark mass thus tuned is checked against  $D_s$  meson, making use of the  $c$ -quark mass obtained above and found to agree with the experimental  $D_s$  (1968 MeV).

TABLE V.  $D$  and  $B$  meson masses in MeV with the tuned  $am_b, am_c$  and  $am_s$ .

$L^3 \times T$	$B_c$	$D_s$	
		$\eta_s$	$B_s$
$16^3 \times 48$	6260(8)	1994(3)	2197(2)
$20^3 \times 64$	6263(12)	1977(4)	2172(2)
$28^3 \times 96$	6255(10)	1971(3)	2167(2)
PDG [8]	6275	1968	

Next we explore, tuning  $m_s$  when  $s$ -quark is in a bound state with a heavy  $b$  quark. Here we are assuming that the potential experienced by the  $s$  quark in the field of  $b$  quark in  $B_s$  meson remains the same in other strange bottom baryons and there is no spin-spin interactions taking place between the quarks. In the infinite mass limit, the HQET Lagrangian becomes invariant under arbitrary spin rotations [34]. Thereby, we can argue that for  $sbb$  and  $scb$  systems the spin-spin interactions do not contribute significantly in spectrum calculation. However, this argument is perhaps not valid in systems like  $bss$  or  $bsd$  but still with  $s$  quark thus tuned, we possibly can obtain their masses close to their physical masses without resorting to any extrapolation.

In this paper, we will present our results obtained at these two different values of  $m_s$ . In Table (IV) we listed these values of  $s$ -quark masses. In the Table (V) we calculate  $B_c$  and  $D_s$  mesons using tuned  $b$ ,  $c$  and  $s$  masses. As is seen, when  $m_s$  is tuned with  $\eta_s$  the  $D_s$  mass obtained is fairly close to PDG value whereas when tuned to  $B_s$  we see an upward shift by an average 200 MeV. We have observed similar differences when  $s$ -quark appears together with  $c$  in  $(scb)$ -baryon masses.

**$u/d$  quarks:** For the valence  $u/d$  quark mass, we used a range of bare quark masses varying from the lightest sea quark masses all the way to a little above where  $s$  mass is tuned to  $B_s$ . Whenever the mass of a bottom baryon containing  $u/d$  quark(s) is quoted, it will corre-

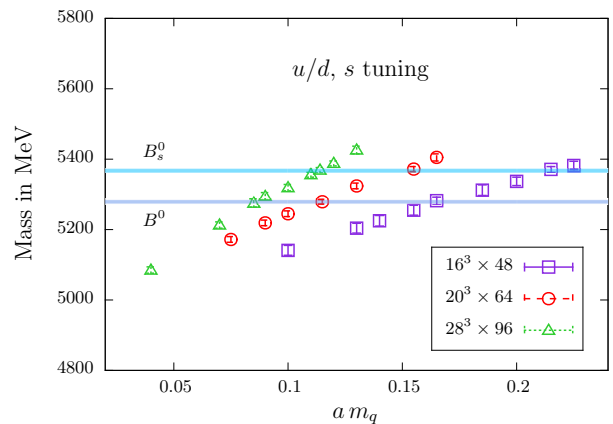


FIG. 1. Tuning of  $s$  and  $u/d$  quark masses in various lattices. The experimental values of  $B^0$  and  $B_s^0$  are shown by bands whose thickness are to enhance visibility and have nothing to do with experimental errors.

spond to  $u/d$  quark mass tuned at  $B$  mass. Since we are not including either electromagnetic or isospin breaking in our calculation, we do not distinguish between  $u$  and  $d$  quarks and it is always  $am_u = am_d$ . This tuning of  $u/d$  mass to  $B$  works well in capturing the  $b$ -baryon states containing single  $u/d$ , such as  $(usb)$  or  $(ucb)$  baryons, when compared to either PDG or other works.

In Table (VI), we listed  $u/d$  quark masses ( $am_q$ ) against the lattice spacing. We show in the Figure 1 our strategy used to tune  $m_s$  and  $m_{u/d}$ .

TABLE VI. Values of  $am_{u/d}$  used in this work.

$L^3 \times T$	$am_{u/d}$
$16^3 \times 48$	0.065, 0.10, 0.13, 0.14, 0.155
(0.15 fm)	0.165, 0.185, 0.215, 0.225
$20^3 \times 64$	0.05, 0.075, 0.090, 0.10,
(0.12 fm)	0.115, 0.13, 0.155, 0.165
$28^3 \times 96$	0.04, 0.07, 0.085, 0.09,
(0.09 fm)	0.10, 0.114, 0.12, 0.13

The tuned  $am_{u/d}$  for different lattices to use with  $b$  quarks are,

$$16^3 \times 48 : 0.165 \quad 20^3 \times 64 : 0.115 \quad 28^3 \times 96 : 0.085$$

The  $s$  and  $u/d$  masses so tuned,  $m_s/m_{u/d}$  turns out to be  $\sim 1.3$  compared to  $\sim 6$  that we get when  $m_s$  is obtained from  $\eta_s$  and  $m_{u/d}$  is the bare sea quark mass.

For states containing two  $u/d$  quarks, such as  $\Sigma_b$  ( $uub$ ) and  $\Lambda_b$  ( $udb$ ), we have mixed success with the above approach. When  $b$  and  $u$  form diquarks ( $QC\gamma_{\{k,5\}}u$ ) for  $\Sigma_b$  state, the masses obtained are consistent with other lattice studies. However, this tuning scheme involving  $B$  fails for  $\Lambda_b$  where the diquark part is  $(uC\gamma_5 d)$  (see the Table II). Hence for  $\Lambda_b$ , containing both  $u$  and  $d$  quarks,

we have to resort to different tuning to account for 190 MeV of mass difference with  $\Sigma_b$ . The mass of  $\Lambda_b$  is obtained from this specially tuned  $m'_{u/d}$  (to be used only for  $\Lambda_b$ ). Thus tuned differently, the mass differences  $\Xi_b - \Lambda_b$  and  $\Sigma_b^* - \Lambda_b$  are well within  $2\sigma$  of PDG values while  $\Lambda_b - B$  is about 60 MeV higher, see the Table (XIV).

## V. RESULTS AND DISCUSSION

In order to extract the masses of the bottom baryons, we perform two-exponential uncorrelated fit to the two-point functions. We then cross-checked it with fitting the effective masses over the same range of time slices. However, this zero momentum energy does not directly give us the mass of the bottom baryons because of unphysical shift in zero of energy. To account for it, the mass is obtained considering energy splittings,

$$M_{\text{latt}} = E_{\text{latt}} + \frac{n_b}{2} (M_{\text{phys}}^{\text{mod}} - E_{\text{latt}}^{\eta_b}) \quad (41)$$

where  $E_{\text{latt}}$  is the lattice zero momentum energy in MeV,  $n_b$  is the number of  $b$ -quarks in the bottom baryon. For bottom mesons ( $b\bar{l}$ ),  $n_b$  is obviously always 1. As discussed before,  $M_{\text{phys}}^{\text{mod}}$  is the modified spin average mass of  $\Upsilon$  and  $\eta_b$  and is equal to 9450 MeV and  $M_{\text{latt}}$  is the lattice bottom baryon mass in MeV.

In calculation of mass splittings this shift in energies is cancelled by subtraction among energies of hadrons having equal number of  $b$  quarks ( $n_b$ ) in them. For this calculation, we use jack-knifed ratio of the correlation functions for fitting [35],

$$C^{Y-X}(t) = \frac{C^Y(t)}{C^X(t)} \sim e^{-(M_Y - M_X)t} \quad (42)$$

Below in the Figure 2 we show a few correlators for single  $b$  baryons containing exclusively either two  $c$  or  $s$  or  $u/d$ .

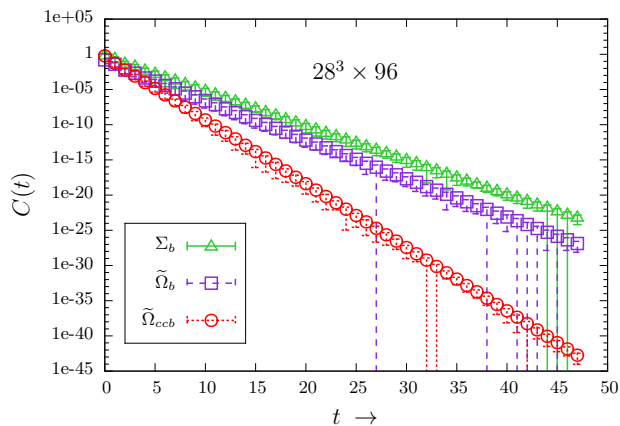


FIG. 2.  $\Sigma_b$ ,  $\tilde{\Omega}_b$  and  $\tilde{\Omega}_{ccb}$  correlators in  $28^3 \times 96$  lattice.

The fitting range is typically chosen (i) looking at positions of what we consider plateau in the effective mass

plots and (ii) exponential fits of the correlators. Both fittings return same masses over suitably chosen range. In the effective mass plot Figure 3, the zero momentum energies and the errors of the same three states as in the Figure 2 are represented as bands.

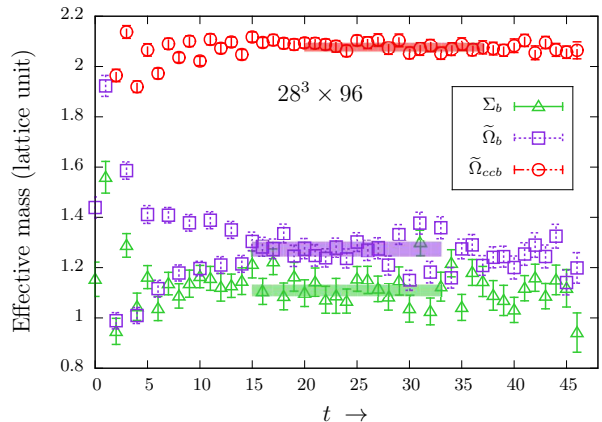


FIG. 3. Effective mass plots for the states in Figure 2. The bands are placed over what we consider plateau.

In these figures, we choose to present the data from  $28^3 \times 96$  lattices but the data from  $16^3 \times 48$  and  $20^3 \times 64$  are similar. Just to remind, in order to obtain the masses in MeV from these, we need the Equation (41).

**Single bottom baryons:** A couple of baryon states containing one  $b$  quark have been listed in the PDG [8], such as  $\Lambda_b$  ( $udb$ ),  $\Omega_b$  ( $ssb$ ),  $\Xi'_b$  ( $usb$ ) etc. and they provide a good matching opportunity. In the Figure 4, we show the agreement of some of these baryon masses with PDG at the tuned  $m_{u/d}$  and  $m_s$ .

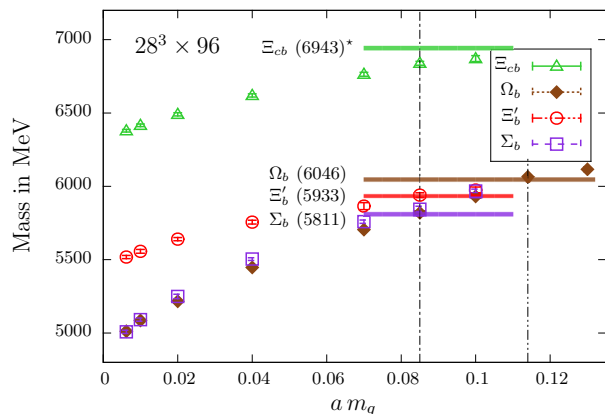


FIG. 4. Variation of single  $b$  baryon masses in MeV against the same light quark masses as in Figure 1.  $m_q = 0.085$  and  $0.114$  are the tuned  $u/d$  and  $s$  quark masses respectively, indicated by dashed vertical lines. The bands correspond to the PDG values, except for  $\Xi_{cb}$  which is taken from [11].

In the following Tables VII, VIII, X and XI, we present



our results of the single and multi  $b$  baryon states corresponding to the operators given in the Tables I and II. In the columns corresponding to various lattice ensembles, we show the masses in lattice unit,  $aE_{\text{latt}}$  of the Equation (41). In the last column of each table, we provide the average  $M_{\text{latt}}$  and the statistical errors, calculated assuming the lattice configurations of different lattice spacings are statistically uncorrelated. Additionally we include tables for  $M_{\text{latt}}$  for the bottom baryons for each lattice spacing in the Appendix.

We collect our results for single bottom baryon, not containing  $s$ -quark(s), in the Table VII and those with  $s$ -quark in Table VIII. For the  $m_{u/d}$ , we state the results when the valence  $m_l$  gives physical  $B$  meson mass.

TABLE VII. Masses, in lattice unit, of baryons involving single  $b$  quark and no  $s$  quark. The bare  $u/d$ -quark masses are 0.165 for  $16^3 \times 48$ , 0.115 for  $20^3 \times 64$  and 0.085 for  $28^3 \times 96$ .

Baryons	$16^3 \times 48$ (0.15 fm)	$20^3 \times 64$ (0.12 fm)	$28^3 \times 96$ (0.09 fm)	Average (MeV)
$\tilde{\Omega}_{ccb}^*$	2.954(5)	2.497(4)	2.088(3)	7807(11)
$\tilde{\Omega}_{ccb}$	2.933(5)	2.482(3)	2.078(3)	7780(9)
$\Omega'_{ccb}$	2.952(4)	2.497(3)	2.078(3)	7797(11)
$\tilde{\Xi}_{cb}^*$	2.222(6)	1.899(4)	1.648(6)	6835(20)
$\Xi_{cb}$	2.177(11)	1.881(4)	1.623(5)	6787(12)
$\tilde{\Xi}_{cb}$	2.199(8)	1.886(4)	1.631(4)	6805(16)
$\Xi'_{cb}$	2.227(6)	1.904(4)	1.653(6)	6843(19)
$\tilde{\Sigma}_b^*$	1.468(8)	1.292(5)	1.189(5)	5836(22)
$\tilde{\Sigma}_b$	1.460(7)	1.290(3)	1.174(6)	5820(21)
$\Sigma'_b$	1.470(7)	1.305(3)	1.194(9)	5848(18)
$\Lambda_b$	1.322(7)	1.208(6)	1.109(9)	5667(14)

Since  $s$  quark has been tuned in two different ways, we quote both the  $b$ -baryon masses at  $\eta_s$ ,  $B_s$  points.

As is evident from our results, the numbers coming from  $s$ -quark tuned to  $\eta_s$  are about 300 MeV smaller from those tuned to  $B_s$  (600 MeV in baryons with two  $s$ ). If we take  $\Omega_b$  ( $ssb$ ) and compare with PDG value 6046 MeV, it becomes obvious.

Next we determine mass differences in single bottom sector including the hyperfine splittings.

The mass splittings are calculated using ratio of correlators as given in the Equation (42). As an example, in the Figure 5 we provide the plots for ratio of correlators,  $\Omega'_b - \Lambda_b$  and  $\Xi_b - \Lambda_b$ , for comfortable viewing because of their relatively large mass differences *i.e.* slopes are prominent and well separated. In case of smaller differences, for instance  $\tilde{\Omega}_b^* - \tilde{\Omega}_b$  or  $\tilde{\Xi}_{cb}^* - \tilde{\Xi}_{cb}$ , the slopes of the ratio of correlators are rather small and not quite visible. In the Table IX above we collect the results of single  $b$  baryons mass splittings.

Heavy quark basically acts as a static color source, and therefore, we expect that the hyperfine splittings between states containing single or multiple  $s$  and  $u/d$  quark(s) to depend only weakly on the tuning of  $m_s$  and

TABLE VIII. Masses, in lattice unit, of baryons containing single  $b$ -quark and  $s$ -quark(s).

Baryons	Tuning	$16^3 \times 48$ (0.15 fm)	$20^3 \times 64$ (0.12 fm)	$28^3 \times 96$ (0.09 fm)	Average (MeV)
$\tilde{\Omega}_{cb}^*$	$\eta_s$	2.035(5)	1.782(5)	1.542(3)	6611(9)
	$B_s$	2.292(7)	1.957(6)	1.693(4)	6930(19)
$\Omega_{cb}$	$\eta_s$	2.010(8)	1.754(5)	1.532(3)	6578(9)
	$B_s$	2.248(11)	1.937(7)	1.684(2)	6893(16)
$\tilde{\Omega}_{cb}$	$\eta_s$	2.012(7)	1.765(5)	1.536(3)	6587(10)
	$B_s$	2.267(8)	1.943(7)	1.686(2)	6906(17)
$\Omega'_{cb}$	$\eta_s$	2.052(5)	1.785(5)	1.548(3)	6625(8)
	$B_s$	2.297(6)	1.966(6)	1.705(2)	6946(17)
$\tilde{\Xi}_b^*$	$\eta_s$	0.987(4)	0.945(2)	0.918(3)	5237(8)
	$B_s$	1.541(8)	1.352(6)	1.235(6)	5935(22)
$\Xi_b$	$\eta_s$	0.986(5)	0.947(2)	0.909(4)	5231(11)
	$B_s$	1.520(9)	1.345(3)	1.207(6)	5901(20)
$\tilde{\Xi}_b$	$\eta_s$	0.978(5)	0.944(2)	0.904(5)	5222(13)
	$B_s$	1.532(11)	1.350(4)	1.224(4)	5921(19)
$\Xi'_b$	$\eta_s$	0.987(4)	0.948(3)	0.913(5)	5235(11)
	$B_s$	1.544(10)	1.366(4)	1.238(6)	5946(16)
$\tilde{\Omega}_b^*$	$\eta_s$	1.129(5)	1.058(3)	1.012(4)	5430(11)
	$B_s$	1.611(8)	1.412(6)	1.264(3)	6019(20)
$\tilde{\Omega}_b$	$\eta_s$	1.118(7)	1.050(3)	0.997(4)	5410(10)
	$B_s$	1.600(11)	1.411(7)	1.264(3)	6014(17)
$\Omega'_b$	$\eta_s$	1.131(9)	1.057(3)	1.007(2)	5427(9)
	$B_s$	1.615(8)	1.425(7)	1.295(2)	6051(15)

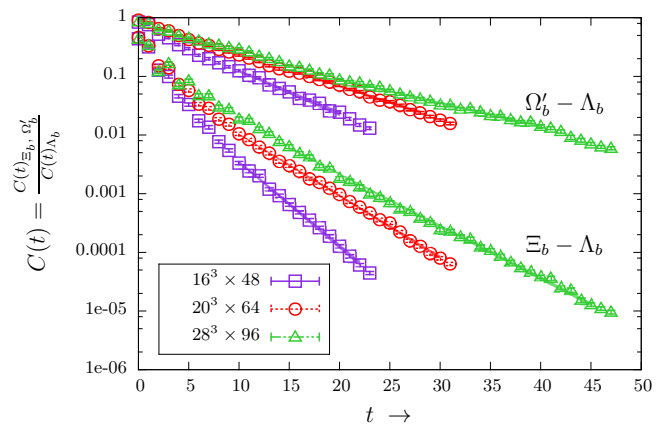


FIG. 5. Ratio of correlators for the calculation of the two splittings shown in Table IX. The bands overlaid on the data points represent single exponential fits.

$m_{u/d}$ . For  $m_{u/d} \leq 0.085$  and two values of  $m_s$  we show this pattern for a few hyperfine splittings in Figure 6.

**Double bottom baryons:** For the baryons containing more than one  $b$ -quark, the data are relatively less noisy than those containing single  $b$ . The effective mass plots

TABLE IX. Single bottom baryons mass splittings in MeV.

Baryon splittings	$16^3 \times 48$ (MeV)	$20^3 \times 64$ (MeV)	$28^3 \times 96$ (MeV)	Average (MeV)
$\tilde{\Omega}_{ccb}^* - \tilde{\Omega}_{ccb}$	28(3)	23(2)	–	26(3)
$\tilde{\Omega}_{cb}^* - \tilde{\Omega}_{cb}$	59(8)	62(13)	61(22)	61(15)
$\tilde{\Xi}_{cb}^* - \tilde{\Xi}_{cb}$	37(6)	44(5)	44(9)	42(7)
$\tilde{\Omega}_b^* - \tilde{\Omega}_b$	29(5)	28(11)	29(4)	29(7)
$\Omega_b' - \Lambda_b$	396(4)	391(9)	406(10)	398(9)
$\tilde{\Xi}_b^* - \Xi_b$	138(20)	122(38)	138(46)	133(36)
$\tilde{\Xi}_b - \Lambda_b$	170(9)	166(11)	163(6)	166(9)
$\Lambda_b - B$	391(20)	431(20)	397(22)	406(21)
$\tilde{\Sigma}_b^* - \tilde{\Sigma}_b$	30(9)	30(8)	29(8)	30(8)
$\tilde{\Sigma}_b^* - \Lambda_b$	224(13)	203(12)	175(13)	201(13)

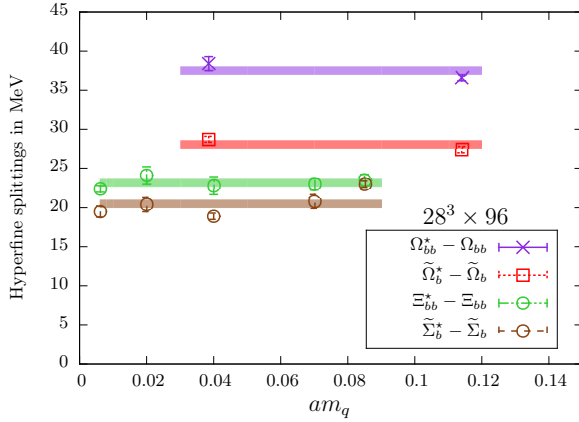


FIG. 6. Hyperfine splittings at various  $m_s$  and  $m_{u/d}$  for a selected few bottom baryons on  $28^3 \times 96$  lattice. Horizontal bands are the average values of the splittings and is used to guide the eye.

in Figure 7, shown for only  $16^3 \times 48$  lattices but similar for two other lattices, is an evidence for this. The fitting ranges are chosen the same way as is done for Figure 3. The plot for  $\Omega_{bbb}^*$  appears counter intuitive since being the heaviest, it is showing lower mass compared to the other two. However, it receives large correction because of shift in rest mass of three  $b$ -quarks.

We tabulate our results for double bottom non-strange baryons in the Table X while those containing  $s$  quark in Table XI.

It is to note that  $\Omega_{bbb}$  is a spin-3/2 state having no spin-1/2 counterpart. But in practice we can take a spin-1/2 projection to get such a fictitious state. Therefore, we label the physical ( $bbb$ ) spin-3/2 state with  $\Omega_{bbb}^*$  to keep consistency with our remaining notation. In this case none of the states have PDG entries.

We would like to point out that the variation of the  $\Xi_{bb}$  ( $ubb$ ) masses with  $m_{u/d}$  is almost absent as the major contribution to these baryons are coming from the two  $b$  quarks. Similarly, from the Table XI we see that

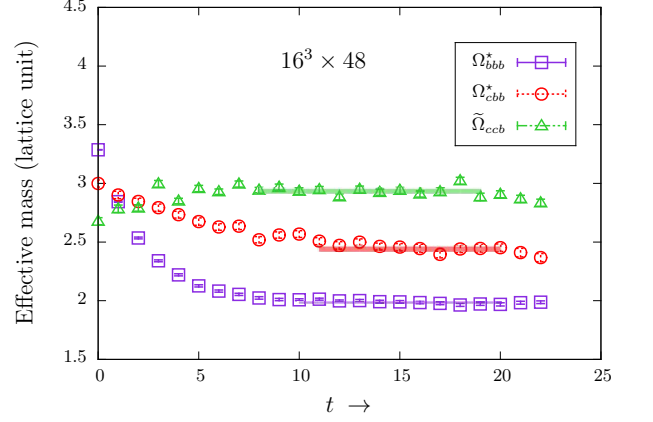


FIG. 7.  $\Omega_{bbb}^*$ ,  $\tilde{\Omega}_{cbb}^*$  and  $\tilde{\Omega}_{ccb}^*$  effective masses.

TABLE X. Triple and double bottom non-strange baryon masses.

Baryon	$16^3 \times 48$ (0.15 fm)	$20^3 \times 64$ (0.12 fm)	$28^3 \times 96$ (0.09 fm)	Average (MeV)
$\Omega_{bbb}^*$	1.983(4)	2.031(3)	2.154(4)	14403(7)
$\Omega_{bbb}$	1.974(4)	2.023(5)	2.148(4)	14390(8)
$\Omega_{cbb}^*$	2.429(16)	2.259(4)	2.117(3)	11081(21)
$\Omega_{cbb}$	2.409(16)	2.246(5)	2.110(3)	11060(23)
$\tilde{\Omega}_{cbb}^*$	2.431(8)	2.255(4)	2.113(3)	11077(14)
$\tilde{\Omega}_{cbb}$	2.432(10)	2.251(4)	2.113(3)	11075(13)
$\Omega'_{cbb}$	2.434(8)	2.250(4)	2.114(4)	11076(12)
$\Xi_{bb}^*$	1.721(12)	1.643(10)	1.666(5)	10103(24)
$\Xi_{bb}$	1.700(12)	1.640(7)	1.664(5)	10091(17)
$\tilde{\Xi}_{bb}^*$	1.720(12)	1.635(8)	1.668(3)	10100(27)
$\tilde{\Xi}_{bb}$	1.703(16)	1.634(8)	1.661(4)	10087(22)
$\Xi'_{bb}$	1.704(16)	1.635(10)	1.672(3)	10096(24)

the different tuning of  $s$  quark has significantly less influence on the double bottom baryon masses, a situation unsurprisingly similar to double bottom baryons with a  $u/d$  quark.

The splittings in double bottom sector is tabulated in the Table XII.

In the double bottom sector, the splittings between the spin-3/2 and 1/2 states are particularly interesting because HQET relates this mass differences with hyperfine splittings of heavy-light mesons, which in the heavy-quark limit [37]

$$\frac{\Delta M_{bb}^{\text{baryon}}}{\Delta m_b^{\text{meson}}} \rightarrow \frac{3}{4} \quad (43)$$

This behavior is consistent with our results within errors as can be seen in Table XIII.

A few GMO mass relations involving  $b$ -quark are provided in the reference [36], which we try to verify in this

TABLE XI. Double bottom strange baryon spectra.

Baryon	Tuning	$16^3 \times 48$ (0.15 fm)	$20^3 \times 64$ (0.12 fm)	$28^3 \times 96$ (0.09 fm)	Average (MeV)
$\Omega_{bb}^*$	$\eta_s$	1.545(11)	1.536(6)	1.576(4)	9902(12)
	$B_s$	1.791(12)	1.703(11)	1.716(3)	10203(22)
$\Omega_{bb}$	$\eta_s$	1.553(9)	1.527(7)	1.570(4)	9896(13)
	$B_s$	1.768(12)	1.699(8)	1.715(3)	10190(17)
$\tilde{\Omega}_{bb}^*$	$\eta_s$	1.542(9)	1.529(7)	1.575(4)	9896(12)
	$B_s$	1.791(12)	1.693(10)	1.717(3)	10199(28)
$\tilde{\Omega}_{bb}$	$\eta_s$	1.541(12)	1.527(7)	1.571(4)	9891(13)
	$B_s$	1.789(9)	1.695(7)	1.714(3)	10197(24)
$\Omega'_{bb}$	$\eta_s$	1.552(9)	1.539(7)	1.578(3)	9908(11)
	$B_s$	1.782(9)	1.699(7)	1.720(3)	10200(20)

TABLE XII. Double bottom baryon mass splittings in MeV. None of the splittings have PDG entries.

Baryon splittings	$16^3 \times 48$ (MeV)	$20^3 \times 64$ (MeV)	$28^3 \times 96$ (MeV)	Average (MeV)
$\tilde{\Omega}_{cbb}^* - \tilde{\Omega}_{cbb}$	–	25(5)	35(2)	30(5)
$\Omega_{bb}^* - \Omega_{bb}$	34(5)	25(8)	37(9)	32(7)
$\Xi_{bb}^* - \Xi_{bb}$	–	25(4)	39(7)	32(5)

work,

$$M_{\Omega_{ccb}^*} - M_{\Omega_{ccb}} \approx M_{\tilde{\Omega}_{cbb}^*} - M_{\tilde{\Omega}_{cbb}} \quad (44)$$

$$M_{\Sigma_b^*} - M_{\Sigma_b} \approx M_{\Xi_{bb}^*} - M_{\Xi_{bb}} \quad (45)$$

For the GMO relation (44), the both sides are expected to be approximately 31 MeV. In our case for  $20^3 \times 64$  lattice, for which we have data for both the sides, they are approximately equal but is around 24 MeV as against 31 MeV given in [36]. Our lattice data is also consistent with the approximate GMO relation (45), where each side is about 30 MeV against 20 MeV calculated in [36].

## VI. SUMMARY

In this paper we presented lattice QCD determination of masses of the baryons containing one or more  $b$  quark(s) using NRQCD action for the  $b$ -quark and HISQ action for the  $c$ ,  $s$  and  $u/d$  quarks. This combination of NRQCD and HISQ has previously been employed in [24] for bottom mesons, however, the exact implementation was rather different. In this work, we converted the one component HISQ propagators to  $4 \times 4$  matrices by the Kawamoto-Smit transformation and the two component NRQCD propagators to  $4 \times 4$  matrices using the prescription suggested in [11].

We have discussed the construction of one and two bottom baryon operators in details and pointed out the difficulty for constructing operators motivated by HQET

TABLE XIII. Ratio of hyperfine splittings of doubly heavy baryons to heavy mesons in the heavy quark limit in  $28^3 \times 96$  lattice.

Baryon splittings	Our results (MeV)	Meson splittings	Our results (MeV)	Ratio
$\tilde{\Omega}_{bbc}^* - \tilde{\Omega}_{bbc}$	35(2)	$B_c^* - B_c$	46(4)	0.76(4)
$\Omega_{bb}^* - \Omega_{bb}$	37(9)	$B_s^* - B_s$	45(9)	0.82(9)
$\Xi_{bb}^* - \Xi_{bb}$	39(7)	$B^* - B$	47(7)	0.83(8)

for single bottom baryons. Consequently, we modified the operators accordingly. For some of the baryons, we have multiple operators for the same state *i.e.* baryons having the same quantum numbers. It would be natural in such cases to construct correlation matrices and obtain lowest lying *i.e.* ground states by solving the generalized eigenvalue method.

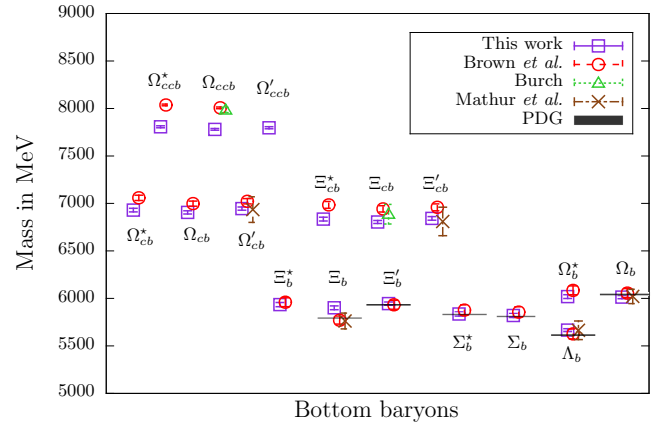


FIG. 8. Comparison of our single bottom baryon spectra with Brown *et al.* [11], Burch [10], Mathur *et al.* [6] and PDG [8] where available.

Single bottom baryons can have isodoublets with the same overall quantum numbers  $J^P$ . For instance, there exist three isodoublets of  $\Xi_b$  which are not radially or orbitally excited states [38]. These states have been categorized by the spin of the  $us$  or  $ds$  diquark denoted by  $j$  and the spin-parity of the baryon. These baryons are referred to as  $\Xi_b(j=0, J^P = \frac{1}{2}^+)$ ,  $\Xi'_b(j=1, J^P = \frac{1}{2}^+)$  and  $\Xi_b^*(j=1, J^P = \frac{3}{2}^+)$ . The same pattern is observed in  $\Xi_c$  states [8]. The mass difference between  $\Xi'_b$  and  $\Xi_b$  is about 150 MeV. So depending upon the choice of the wave function having the same overall quantum numbers we can have different baryon states. If we choose  $(s^T C \gamma_5 d) Q$  as our  $j=0$  baryon operator then we will be simulating  $\Xi_b$  state and if we project out the spin-1/2 state of  $j=1$  operator  $(s^T C \gamma_k d) Q$  then we will get the  $\Xi'_b$ . For reason discussed before, we can not define  $j=1$  light-light diquark state. In our case, the wave function that corresponds to  $\Xi_b^*$  is  $(Q^T C \gamma_5 s) d$ . Constructing operator in this way allows the  $s$  and  $d$  quarks to have paral-

lel spin configurations. By simple physical reasoning we can argue that explicit construction of  $j = 0$  diquark for  $\Xi_b$  is more likely to have significant overlap with physical  $\Xi_b$  compared to  $\Xi'_b$  ( $j = 1$ ) upon gauge averaging. However the operator  $(Q^T C \gamma_5 s) d$  is expected to have a good overlap with  $\Xi'_b$  state and this is also supported by our result. For anti-parallel  $s$  and  $d$  spin configuration,  $\Xi'_b$  can also have an overlap with the  $\Xi_b$  state. On lattice, operators for states having same quantum numbers can mix and, therefore, a detailed GEVP analysis can only resolve the issue of mutual overlap of  $\Xi_b$  and  $\Xi'_b$  states, which we did not include in this work. This is perhaps the reason we see discrepancies in their values with PDG and others in the Figure 8.

The  $b$  mass has been tuned to modified  $\Upsilon - \eta_b$  spin average mass while  $c$  quark to  $J/\psi - \eta_c$  spin average mass. The  $s$  quark required to be tuned to both the fictitious  $\eta_s$  and  $B_s$  mass since we expect the bottom-strange bound state to be more appropriate than  $s - \bar{s}$  bound state in bottom baryons. For the light  $u/d$  quarks, we have considered a wide range of bare masses and tune it using  $B$  meson. However, this scheme of tuning  $u/d$  quarks has not worked for  $\Lambda_b$ . There  $u/d$  are tuned to capture the 150 MeV mass difference  $\Sigma_b - \Lambda_b$ . This specially tuned  $m'_{u/d}$ , which is used only for  $\Lambda_b$ , gives it a mass of 5667 MeV. The PDG value for  $\Lambda_b$  mass is 5620 MeV. We demonstrated the variation of bottom baryons as well as hyperfine splittings against varying  $m_s$  and  $m_{u/d}$ . We showed that the hyperfine splittings are almost independent of  $s$  and  $u/d$  quark masses.

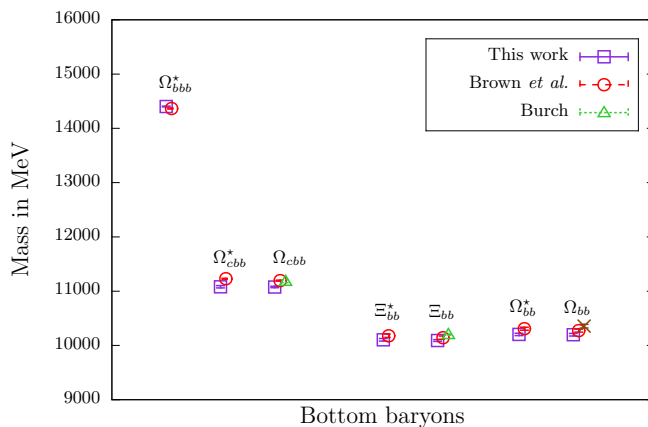


FIG. 9. Comparison of our triple and double bottom baryon spectra with Brown *et al.* [11] and Burch [10].

We compare our bottom baryon results with other works, mostly with [6, 10, 11], in the Figures 8 and 9. NRQCD has been standard action of choice for  $b$  quark in these three cited studies, but the actions used for  $c$  are all different – NRQCD, Clover-Wilson and relativistic heavy quark action [39]. Whatever differences we see in the results for single  $b$  baryons with  $c$  quark, particularly in the cases with two  $c$ , possibly have stemmed from the differences in actions. However, in this work

we do not address the systematics involved, which could be significant, because of these differences. (The study of such systematics needed to arrive at phenomenologically relevant numbers will be reported elsewhere.) But otherwise, the results of bottom baryon spectra in the present study with NRQCD  $b$  quark and HISQ  $c, s, u/d$  quarks appear to agree with each other. We would like to emphasize again that the errors we reported here are only statistical.

The comparison of the hyperfine splittings is shown in the Figure 10.

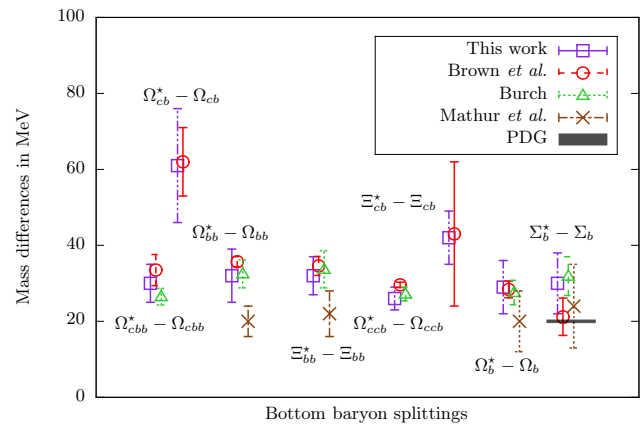


FIG. 10. Hyperfine splittings of bottom baryons calculated in this work and compared with Brown *et al.* [11], Burch [10], Mathur *et al.* [6] and PDG [8] where available.

Apart from the hyperfine splittings, a few other mass splittings calculated in this work are assembled in the Table XIV. The bottom baryon spectra and various mass splittings reported in this paper and those appearing in [8, 11] are well comparable given the wide choice of actions and tuning employed in achieving them.

TABLE XIV. Bottom baryon mass differences in MeV. PDG values without error is simply the differences of the two states.

Mass splittings	This work	Brown <i>et al.</i> [11]	PDG [8]
$\Omega'_b - \Lambda_b$	398(9)	–	426.4(2.2)
$\Xi^*_b - \Xi_b$	133(36)	189(29)	155.5
$\Xi_b - \Lambda_b$	166(9)	–	172.5(0.4)
$\Lambda_b - B$	406(21)	–	339.2(1.4)
$\Sigma^*_b - \Lambda_b$	201(13)	251(46)	213.5

## VII. ACKNOWLEDGEMENT

The numerical part of this work has been performed at HPC facility in NISER (Kalinga cluster) funded by Dept. of Atomic Energy (DAE), Govt. of India. A significant part of this work has been carried out in

Proton cluster funded by DST-SERB project number SR/S2/HEP-0025/2010. The authors acknowledge useful discussions with Dipankar Chakrabarti (IIT-Kanpur,

India) and Stefan Meinel (University of Arizona, USA) on bottom baryon operator construction. One of the authors (PM) thanks DAE for financial support.

### Appendix: Bottom baryon masses in MeV

For the reason of completeness, we provide the bottom baryon masses in MeV for different lattices used in this work. In these tables we provide only  $B_s$  tuned strange bottom baryon masses and not  $\eta_s$  tuned values.

TABLE XV. Single bottom baryon masses in MeV, corresponding to the Tables VII and VIII.

Baryons	$16^3 \times 48$ (0.15 fm)	$20^3 \times 64$ (0.12 fm)	$28^3 \times 96$ (0.09 fm)	Average	Baryons	$16^3 \times 48$ (0.15 fm)	$20^3 \times 64$ (0.12 fm)	$28^3 \times 96$ (0.09 fm)	Average
$\tilde{\Omega}_{ccb}^*$	7816(6)	7794(6)	7805(6)	7807(11)	$\tilde{\Omega}_{cb}^*$	6945(9)	6906(10)	6938(9)	6930(19)
$\tilde{\Omega}_{ccb}$	7788(6)	7769(5)	7782(6)	7780(9)	$\Omega_{cb}$	6887(14)	6873(11)	6919(4)	6893(16)
$\Omega'_{ccb}$	7813(5)	7794(5)	7782(6)	7797(11)	$\tilde{\Omega}_{cb}$	6912(10)	6883(11)	6923(4)	6906(17)
$\tilde{\Xi}_{cb}^*$	6853(8)	6810(6)	6840(13)	6835(20)	$\Omega'_{cb}$	6951(8)	6921(10)	6965(4)	6946(17)
$\Xi_{cb}$	6794(14)	6781(6)	6785(11)	6787(12)	$\tilde{\Xi}_b^*$	5957(10)	5911(10)	5934(13)	5935(22)
$\tilde{\Xi}_{cb}$	6822(10)	6789(6)	6802(9)	6805(16)	$\Xi_b$	5929(12)	5900(5)	5873(13)	5901(20)
$\Xi'_{cb}$	6859(8)	6819(6)	6851(13)	6843(19)	$\tilde{\Xi}_b$	5945(14)	5908(7)	5910(9)	5921(19)
$\tilde{\Sigma}_b^*$	5861(10)	5812(8)	5833(11)	5836(22)	$\Xi'_b$	5961(13)	5934(7)	5941(13)	5946(16)
$\tilde{\Sigma}_b$	5850(9)	5809(5)	5800(13)	5820(21)	$\tilde{\Omega}_b^*$	6049(10)	6010(10)	5998(7)	6019(20)
$\Sigma'_b$	5864(9)	5834(5)	5844(20)	5848(18)	$\tilde{\Omega}_b$	6035(14)	6008(11)	5998(7)	6014(17)
$\Lambda_b$	5669(9)	5674(10)	5658(20)	5667(14)	$\Omega'_b$	6054(10)	6031(11)	6066(4)	6051(15)

TABLE XVI. Triple and double bottom baryon masses in MeV, corresponding to the Tables X and XI.

Baryons	$16^3 \times 48$ (0.15 fm)	$20^3 \times 64$ (0.12 fm)	$28^3 \times 96$ (0.09 fm)	Average	Baryons	$16^3 \times 48$ (0.15 fm)	$20^3 \times 64$ (0.12 fm)	$28^3 \times 96$ (0.09 fm)	Average
$\Omega_{bbb}^*$	14399(5)	14405(5)	14403(9)	14403(7)	$\Omega_{bb}^*$	10217(16)	10177(18)	10216(7)	10203(22)
$\Omega_{bbb}$	14388(5)	14392(8)	14390(9)	14390(8)	$\Omega_{bb}$	10187(16)	10171(13)	10214(7)	10190(17)
$\Omega_{cbb}^*$	11056(21)	11091(6)	11095(7)	11081(21)	$\tilde{\Omega}_{bb}^*$	10217(16)	10161(16)	10218(7)	10199(28)
$\Omega_{cbb}$	11029(21)	11070(8)	11080(7)	11060(23)	$\tilde{\Omega}_{bb}$	10214(12)	10164(11)	10212(7)	10197(24)
$\tilde{\Omega}_{cbb}^*$	11058(10)	11085(7)	11086(7)	11077(14)	$\Omega'_{bb}$	10205(12)	10171(11)	10225(7)	10200(20)
$\tilde{\Omega}_{cbb}$	11060(13)	11078(7)	11086(7)	11075(13)					
$\Omega'_{cbb}$	11062(10)	11076(7)	11088(9)	11076(12)					
$\Xi_{bb}^*$	10124(16)	10078(16)	10106(11)	10103(24)					
$\Xi_{bb}$	10097(16)	10073(11)	10102(11)	10091(17)					
$\tilde{\Xi}_{bb}^*$	10123(16)	10065(13)	10111(7)	10100(27)					
$\tilde{\Xi}_{bb}$	10101(21)	10063(13)	10095(9)	10087(22)					
$\Xi'_{bb}$	10102(21)	10065(16)	10119(7)	10096(24)					

[1] C.T.H. Davies, Proc. Sci. LATTICE2011, 019 (2011).  
[2] E. Gamiz, C.T.H. Davies, G.P. Lepage, J. Shigemitsu, and M. Wingate, Phys. Rev. D80, 014503 (2009).  
[3] A. Ali Khan, T. Bhattacharya, S. Collins, C. T. H. Davies, R. Gupta, C. Morningstar, J. Shigemitsu, and J. Sloan, Phys. Rev. D62, 054505 (2000).

[4] R. Woloshyn, Phys. Lett. B476, 309 (2000).  
[5] R. Lewis, N. Mathur, and R.M. Woloshyn, Phys. Rev. D64, 094509 (2001).  
[6] N. Mathur, R. Lewis, and R.M. Woloshyn, Phys. Rev. D66, 014502 (2002).

- [7] Heechang Na and S.A. Gottlieb, Proc. Sci. LATTICE2006, 191 (2006), Proc. Sci. LATTICE2007, 124 (2007), Proc. Sci. LATTICE2008, 119 (2008).
- [8] M. Tanabashi *et al.* (Particle Data Group), Phys. Rev. D98, 030001 (2018) and 2019 update.
- [9] Stefan Meinel, Phys. Rev. D82, 114514 (2010).
- [10] Tommy Burch, arXiv:1502.00675
- [11] Zachary S. Brown, William Detmold, Stefan Meinel, and Kostas Orginos, Phys. Rev. D90, 094507 (2014).
- [12] G.P. Lepage, L. Magnea, C. Nakhleh, U. Magnea, and K. Hornbostel, Phys. Rev. D46, 4052 (1992).
- [13] B.A. Thacker and G.P. Lepage, Phys. Rev. D43, 196 (1991).
- [14] E. Follana, Q. Mason, C. Davies, K. Hornbostel, G. P. Lepage, J. Shigemitsu, H. Trottier, and K. Wong, Phys. Rev. D75, 054502 (2007).
- [15] Aida X. El-Khadra, Andreas S. Kronfeld, and Paul B. Mackenzie, Phys. Rev. D55, 3933 (1997).
- [16] [www.physics.utah.edu/~detar/milc/](http://www.physics.utah.edu/~detar/milc/)
- [17] C.T.H. Davies, K. Hornbostel, A. Langnau, G.P. Lepage, A. Lidsey, J. Shigemitsu, and J. Sloan, Phys. Rev. D50, 6963 (1994).
- [18] C.T.H. Davies, K. Hornbostel, G.P. Lepage, A.J. Lidsey, J. Shigemitsu, and J. Sloan, Phys. Rev. D52, 6519 (1995).
- [19] N. Kawamoto and J. Smit, Nucl. Phys. B192, 100 (1981).
- [20] Howard D. Trottier, Phys. Rev. D55, 6844 (1997).
- [21] A. Bazavov *et al.*, Rev. Mod. Phys. 82, 1349 (2010), hep-lat/0903.3598.
- [22] K. Orginos and D. Toussaint, Phys. Rev. D59, 014501 (1998).
- [23] K. Orginos, D. Toussaint, and R. L. Sugar, Phys. Rev. D60, 054503 (1999).
- [24] Eric B. Gregory, Christine T. H. Davies, Iain D. Kendall, Jonna Koponen, Kit Wong, Eduardo Follana, Elvira Gmiz, G. Peter Lepage, Eike H. Mller, Heechang Na, and Junko Shigemitsu (HPQCD Collaboration), Phys. Rev. D83, 014506 (2011).
- [25] Nikolai Zerf, PoS RADCOR2015, 089 (2015).
- [26] T.C. Hammant, A.G. Hart, G.M. von Hippel, R.R. Horgan, and C.J. Monahan, Phys. Rev. Lett. 107, 112002 (2011).
- [27] R.J. Dowdall, C.T.H. Davies, T.C. Hammant, and R.R. Horgan, Phys. Rev. D86, 094510 (2012).
- [28] Claude Bernard, Tom Burch, Kostas Orginos, Doug Toussaint, Thomas A. DeGrand, Carleton DeTar, Saumen Datta, Steven Gottlieb, Urs M. Heller, and Robert Sugar, Phys. Rev. D64, 054506 (2001).
- [29] C.T.H. Davies, E. Follana, I.D. Kendall, G.P. Lepage, and C. McNeile, Phys. Rev. D81, 034506 (2010).
- [30] M. Wingate, J. Shigemitsu, C.T.H. Davies, G.P. Lepage, and H.D. Trottier, Phys. Rev. D67, 054505 (2003).
- [31] K. C. Bowler, R. D. Kenway, O. Oliveira, D. G. Richards, P. Ueberholz, L. Lellouch, J. Nieves, C. T. Sachrajda, N. Stella, and H. Wittig (UKQCD Collaboration) , Phys. Rev. D54, 3619 (1996).
- [32] J.M. Flynn, F. Mescia, and A.S.B. Tariq, JHEP 0307, 066 (2003).
- [33] Stefan Meinel, William Detmold, C.-J. David Lin, and Matthew Wingate, PoS LAT2009, 105 (2009).
- [34] J.G. Korner, M. Kramer, and D. Pirjol, Prog. Part. Nucl. Phys. 33, 787 (1994).
- [35] Silas R. Beane, Kostas Orginos, and Martin J. Savage, Phys. Lett. B654 (2007) 20-26
- [36] Xin-Zhen Weng, Xiao-Lin Chen, and Wei-Zhen Deng, Phys. Rev. D97, 054008 (2018).
- [37] Nora Brambilla, Antonio Vairo, and Thomas Rösch, Phys. Rev. D72, 034021 (2005).
- [38] R. Aaij *et al.* (LHCb Collaboration), Phys. Rev. Lett. 114, 062004 (2015).
- [39] S. Aoki, Y. Kuramashi, and S. Tominaga, Prog. Theor. Phys. 109, 383 (2003).